J Biomol NMR (2015) 61:275–286
DOI 10.1007/s10858-014-9893-4

ARTICLE

Solid-state NMR of the *Yersinia pestis* outer membrane protein Ail in lipid bilayer nanodiscs sedimented by ultracentrifugation

Yi Ding · L. Miya Fujimoto · Yong Yao · Francesca M. Marassi

Received: 14 November 2014 / Accepted: 20 December 2014 / Published online: 13 January 2015

Abstract Solid-state NMR studies of sedimented soluble proteins has been developed recently as an attractive approach for overcoming the size limitations of solution NMR spectroscopy while bypassing the need for sample crystallization or precipitation (Bertini et al. Proc Natl Acad Sci USA 108(26):10396–10399, 2011). Inspired by the potential benefits of this method, we have investigated the ability to sediment lipid bilayer nanodiscs reconstituted with a membrane protein. In this study, we show that nanodiscs containing the outer membrane protein Ail from *Yersinia pestis* can be sedimented for solid-state NMR structural studies, without the need for precipitation or lyophilization. Optimized preparations of Ail in phospholipid nanodiscs support both the structure and the fibronectin binding activity of the protein. The same sample can be used for solution NMR, solid-state NMR and activity assays, facilitating structure–activity correlation experiments across a wide range of timescales.

Keywords Nanodisc · NMR · Sedimentation · Membrane protein · Ail · Yersinia

Introduction

The preparation of natively folded and active membrane proteins is a key requirement for structural studies aimed at correlating molecular structure with biological function (Zhou and Cross 2013). NMR spectroscopy is particularly well-suited for examining protein structure and dynamics in samples that are very close to their functional environments, and for establishing structure–activity correlations by direct spectroscopic detection of ligand binding events or conformational changes (Shuker et al. 1996). However, while it is relatively straightforward to mimic the homogeneous physical and chemical properties of the isotropic aqueous environment surrounding soluble proteins, reconstituting a heterogeneous environment that mimics the anisotropic properties of the lipid bilayer membrane presents additional challenges. For example, even in cases where detergent micelles support native fold, the interaction of detergents with water-exposed regions of membrane proteins can interfere with ligand-binding activity precluding parallel structure–activity studies aimed at understanding biological function.

Progress on NMR structure determination of membrane proteins is documented in the protein data bank (PDB) and highlighted in the database of membrane proteins structures determined by NMR (http://www.drorlist.com/nmr.html). Solid-state NMR methods can be used for proteins in a variety of lipid sample environments including: liposomes, supported planar lipid bilayers, macrodiscs, lipid-detergent bicelles or precipitated lipid preparations (Drechsler and Separovic 2003; McDermott 2009; Sharma et al. 2010; Maltsev and Lorigan 2011; Park et al. 2011, 2012; Durr et al. 2012; Franks et al. 2012; Hong et al. 2012; Orwick-Rydmark et al. 2012; Ding et al. 2013; Gopinath et al. 2013; Loquet et al. 2013; Mors et al. 2013; Murray et al. 2013; Ni et al. 2013; Tang et al. 2013; Ullrich and Glaubitz 2013; Wang et al. 2013; Weingarth and Baldus 2013; Sackett et al. 2014). Solution NMR studies can be performed on membrane proteins in detergent micelles (Arora and Tamm 2001; Fernandez and Wuthrich 2003; Sanders and Sonnichsen 2006; Chill et al. 2007; Poget and Girvin 2007; Prosser et al. 2007; Teriete et al.

Y. Ding · L. M. Fujimoto · Y. Yao · F. M. Marassi (✉)
Sanford-Burnham Medical Research Institute, 10901 North Torrey Pines Road, La Jolla, CA 92037, USA
e-mail: fmarassi@sbmri.org

2007; Hiller and Wagner 2009; Kim et al. 2009; Zhou et al. 2008; Berardi et al. 2011; Wang and Tjandra 2013; Fox et al. 2014) and, more recently, lipid bilayer nanodiscs are being used effectively for solution NMR studies of membrane proteins (Gluck et al. 2009; Raschle et al. 2009; Shenkarev et al. 2009, 2010; Etzkorn et al. 2013; Hagn et al. 2013; Shenkarev et al. 2013; Tzitzilonis et al. 2013; Bibow et al. 2014; Susac et al. 2014).

The ability to perform NMR studies on one sample in both the solid-state and in solution could extend the range of dynamics and functional properties that can be probed for a given protein. The recent demonstration, by Bertini and coworkers (Bertini et al. 2011, 2012a), that large soluble proteins can be sedimented either in situ, by the G forces active during magic angle spinning (MAS) solid-state NMR experiments, or by ultracentrifugation, before transfer to the MAS rotor, provide an avenue for this approach. As noted by the authors (Bertini et al. 2011), "Ultracentrifuged proteins are usually well behaved. The sediment resolubilizes as soon as the centrifugal force is removed, and the protein generally maintains its native state throughout". Evidence of protein functionality in the sedimented state is provided by equilibrium sedimentation in many studies. Conversely, precipitation and lyophilization can compromise biological function.

Inspired by this work we have examined the ability to sediment nanodiscs, containing the outer membrane protein Ail, for solid-state NMR. Previous solid-state NMR studies of proteins in nanodiscs used precipitation with polyethylene glycol (PEG) or lyophilization to pack nanodisc samples in the limited volume of a MAS rotor (Li et al. 2006; Kijac et al. 2007, 2010; Mors et al. 2013; Boettcher et al. 2011). However, PEG precipitation has been reported to disrupt nanodiscs prepared with certain lipids (Kijac et al. 2010). Furthermore, precipitation and lyophilization are not always compatible with protein activity.

Ail is a virulence factor from *Yersinia pestis*, that mediates bacterial cell adhesion to human cells and endows the bacterium with resistance to human innate immunity. The interactions of *Y. pestis* Ail with the extracellular matrix proteins fibronectin and laminin have been shown to be important for mediating bacterial cell adhesion (Tsang et al. 2010, 2012; Yamashita et al. 2011). Amino acid residues in the protein's four extracellular loops (EL1–EL4) have been shown to play important roles in the adhesion of *Y. pestis* and the related *Yersinia* species *Y. enterocolitica* (Miller et al. 2001; Tsang et al. 2013) as well as in the invasion and serum resistance of *Y. enterocolitica* (Miller et al. 2001).

The crystal structure of Ail has been determined in tetraethylene glycol monooctyl ether (C_8E_4) at high resolution (Yamashita et al. 2011). Ail adopts an eight-stranded β-barrel conformation similar to that of its homolog OmpX. However, several residues in the functionally important loops EL2 and EL3 are disordered and incompletely resolved in the crystal structure, and little is known about the loop-mediated interactions of Ail with its human host partners.

Recently, we assigned the solution NMR spectrum of Ail in *n*-decyl-phosphocholine (DePC) micelles and showed that the protein adopts the correct β-barrel fold in this detergent (Ding et al. 2015). However, we found that the high detergent concentration required for high-resolution NMR spectroscopy is not compatible with ligand binding, precluding NMR mapping experiments aimed at correlating structure with activity. By contrast, the protein embedded in lipid bilayer nanodiscs is fully functional and also yields well-resolved solution NMR spectra. However, these spectra have broader lines and may not be amenable to chemical shift mapping studies with large protein ligands of Ail, such as fibronectin, a large disulfide-linked homodimer of 500 kD subunits.

Here we show that it is possible to sediment phospholipid nanodiscs reconstituted with Ail for solid-state NMR experiments. Optimized preparations of Ail in nanodiscs support both activity and structure, and can be used for parallel activity and NMR studies on exactly the same samples. Sedimentation in an ultracentrifuge yields dense transparent preparations, highly enriched in Ail nanodiscs, that can be used for solid-state NMR experiments and correlating structural and activity information.

Materials and methods

Expression and purification of membrane scaffold proteins

Two variants of the membrane scaffold protein (MSP), needed for nanodisc assembly, were expressed and purified as described previously: MSP1E3D1, which contains three additional helices (repeats of helices 4, 5 and 6) compared to the MSP1D1 sequence (Denisov et al. 2007), and MSP1D1-Δh5, which lacks helix 5 of MSP1D1 (Hagn et al. 2013). The pET-28a MSP1E3D1 plasmid was obtained from Addgene (Addgene plasmid 20066). The nucleotide encoding MSP1D1Δh5 was obtained from GenScript and cloned into plasmid pET-28a (EMD) as described (Ding et al. 2015). The MSPs were purified by Ni-affinity chromatography and the C-terminal His tags were removed by proteolysis with tobacco etch virus.

Expression and purification of Ail

Wild-type Ail and C-terminal His-tagged Ail (Ail-His) were cloned in the *E. coli* plasmid pET-30b, expressed and

purified as described previously (Ding et al. 2015). The expressed amino acid sequences of Ail and Ail-His begin with an extra N-terminal methionine before residue Glu1 of the native sequence. The sequence of Ail terminates with the native residue Phe156, while Ail-His includes 33 additional C-terminal residues from the His tag of the plasmid vector. For ^{15}N and ^{13}C labeling of Ail, bacteria were grown in M9 medium containing 1 g/L of U-99 % $^{15}NH_4Cl$ and 2 g/L of U-99 % ^{13}C-glucose (Cambridge Isotope Laboratories) as the sole sources of N and C atoms.

Preparation and assays of Ail in micelles, vesicles and nanodiscs and functional assays

Ail was refolded in DePC (Anatrace) and samples were prepared for solution NMR in DePC micelles, phospholipid liposomes and phospholipid nanodiscs, as described (Ding et al. 2015). Protein folding was assessed by monitoring the shift in SDS-PAGE apparent molecular weight that correlates with the transition from unfolded to folded states of transmembrane β-barrels (Tamm et al. 2004) and by NMR spectroscopy as illustrated in the text. The DePC concentration was estimated by monitoring the intensity of the ^1H NMR peak from the trimethylamino protons at 3.15 ppm. The optimal Ail/MSP/lipid ratio for Ail-containing nanodiscs was determined as described (Ding et al. 2015), by screening with size exclusion chromatography (Superdex 75 10/300 GL column, GE Healthcare), performed in nanodisc buffer (20 mM Tris–Cl, pH 7.5, 100 mM NaCl, 1 mM EDTA) and monitored by detecting the UV absorbance at 280 nm of Ail and MSP. Enzyme-linked immunosorbent assays (ELISA) were performed as described (Ding et al. 2015), using Ail-His incorporated in MSP1D1Δh5 nanodiscs, MSP1E3D1 nanodiscs or DePC micelles.

Nanodisc sedimentation

Nanodisc sedimentation experiments were performed using a Beckman Airfuge equipped with an A/100-30 rotor, at room temperature and 90,000 rpm (160,000×*g*). The extent of sedimentation was assessed by measuring the UV absorbance at 280 nm (A_{280}) of the supernatant 170 µL fraction and bottom 50 µL fraction, obtained in the 240 µL centrifuge tube.

Samples for NMR spectroscopy

The samples of Ail in micelles contained 0.5 mM Ail (4 mg), 170 mM DePC and NMR buffer (20 mM Na-PO_4, pH 6.8, 5 mM NaCl, 1 mM EDTA, 10 % D_2O), in a volume of 450 µL. The samples of Ail in MSP1D1Δh5 nanodiscs contained 0.5 mM Ail (4 mg), 37.5 mM DMPC (11.5 mg), 12.5 mM DMPG (3.9 mg) and NMR buffer, in a volume of 450 µL. The samples of Ail in sedimented nanodiscs, for solid-state NMR studies, contained 5.5 mM Ail (3.5 mg), 825 mM DMPC (20 mg), 275 mM DMPG (6.8 mg) and NMR buffer, in a volume of 36 µL inside the MAS rotor. The samples of Ail in proteoliposomes for solid-state NMR studies contained 2.4 mM Ail (1.5 mg), 740 mM DMPC (18 mg) and NMR buffer, in a volume of 36 µL inside the MAS rotor.

NMR experiments

Solution NMR experiments were performed on a Bruker AVANCE 600 MHz spectrometer equipped with a $^1H/^{15}N/^{13}C$ triple-resonance cryoprobe. TROSY-based (Pervushin et al. 1997; Salzmann et al. 1998) $^1H–^{15}N$ correlation NMR spectra were obtained with 16 transients for $^2H/^{15}N$ labeled Ail in nanodiscs, or 8 transients for $^2H/^{15}N$ labeled Ail in DePC, for each of 256 *t1* points. Backbone CA and CB chemical shifts were taken from the deposited (BMRB accession: 25281) resonance assignments for Ail in 170 mM DePC (Ding et al. 2015).

Solid-state NMR studies were performed on a Bruker AVANCE 500 MHz spectrometer equipped with a Bruker $^1H/^{15}N/^{13}C$, 4 mm, Efree MAS probe and a home-built $^1H/^{15}N$, 5 mm Efree, static probe, or on a Bruker AVANCE 700 MHz spectrometer equipped with a home-built $^1H/^{15}N/^{13}C$, 3.2 mm, Efree MAS probe.

One-dimensional ^{31}P spectra were acquired using a Hahn echo pulse sequence with continuous wave ^1H decoupling. One-dimensional ^{13}C and ^{15}N spectra were acquired on the 500 and 700 MHz spectrometers, using cross polarization (CP; Pines et al. 1973) or insensitive nuclei enhancement by polarization transfer (INEPT; Morris and Freeman 1979) pulse sequences. CP spectra were obtained with $^1H–^{13}C$ or $^1H–^{15}N$ contact times of 400 µs or 2 ms and TPPM or SWf-TPPM sequences for ^1H decoupling. INEPT ^{15}N spectra were obtained with a magnetization transfer time of 2.5 ms. INEPT ^{13}C spectra were obtained with a transfer time of 1.67 ms and a 1.11 ms refocusing delay.

Two-dimensional solid-state NMR $^{13}C–^{13}C$ correlation spectra were acquired on the 700 MHz spectrometer, using proton driven spin diffusion (PDSD; Szeverenyi et al. 1982), with a $^1H–^{13}C$ contact time of 400 µs, a mixing time of 50 ms and SWf-TPPM ^1H decoupling. A total of 32 transients (sedimented nanodiscs) or 512 transients (proteoliposomes) were acquired for each of 1,024 *t1* points.

The NMR data were processed using NMRPipe (Delaglio et al. 1995) and analyzed using NMRView (Johnson and Blevins 1994).

Results and discussion

Preparation and solution NMR of Ail nanodiscs

Yersinia pestis Ail can be refolded in a variety of detergent and lipid samples suitable for solution and solid-state NMR (Plesniak et al. 2011; Ding et al. 2013, 2015). To examine the usefulness of Ail nanodiscs for structural and ligand-binding activity studies, we prepared two types of samples with different nanodisc sizes. The shorter scaffold protein, MSP1D1Δh5, has been developed specifically for the preparation of smaller nanodiscs to facilitate solution NMR studies of membrane proteins (Hagn et al. 2013). The longer the longer scaffold protein, MSP1E3D1, has been developed for biochemical studies of larger membrane protein and their complexes (Denisov et al. 2007).

Optimal preparations of Ail in MSP1D1Δh5 nanodiscs were obtained with a molar ratio of 1/2/100 (Ail/MSP/phospholipid; Ding et al. 2015). Analysis by size exclusion chromatography (Fig. 1a) shows that they have a narrow elution profile and homogeneity similar to empty nanodiscs. Indeed, ^{15}N labeled Ail incorporated in MSP1D1Δh5 nanodiscs yields a well-dispersed ^{1}H/^{15}N correlation NMR spectrum with many well-resolved peaks of homogeneous intensity (Fig. 1b). Although the ^{1}H and ^{15}N resonance lines are broader than those observed in the spectra of Ail in DePC micelles (Fig. 2b), the nanodisc and micelle spectra also share many similarities, indicating that the protein adopts a similar fold in the two environments. Many peaks, including several from Gly, Trp and Phe residues, appear at nearly identical positions and can be tentatively assigned to specific sites by comparison with the assigned spectrum of Ail in DePC (BMRB accession: 25281).

Homogenous preparations were also obtained for Ail in MSP1E3D1 nanodiscs, at a molar ratio of 1/2/200 (Ail/MSP/phospholipid). Consistent with the larger size of these nanodiscs, size exclusion chromatography shows that they elute significantly faster than their smaller MSP1D1Δh5 counterparts, at an elution volume that is similar to that of empty MSP1E3D1 nanodiscs (Fig. 1a).

The larger size of these nanodiscs prevents protein signals to be detected in the solution NMR spectra of ^{13}C labeled Ail. The ^{13}C INEPT spectrum (Fig. 1c) is dominated by signals from the natural abundance ^{13}C in the phospholipids, while only weak signals from protein aromatic side chain sites are visible. Hydrodynamic diameters in the range of 14 nm have been reported for nanodiscs prepared with MSP1E3D1 (Denisov et al. 2007). The solid-state NMR ^{31}P spectrum of the nanodisc lipids displays a single sharp peak at the isotropic frequency of the lipid and buffer phosphate groups (Fig. 1d). The spectrum shows no sign of the characteristic, motionally averaged powder pattern, that is observed for liquid crystalline phospholipid bilayer assemblies larger than ~ 150 nm (Burnell et al. 1980). These results are consistent with the known effects of phospholipid dynamics on their NMR spectra, as described in an extensive body of seminal papers in this area (Oldfield and Chapman 1971; Birdsall et al. 1972; Levine et al. 1972; Bloom et al. 1977, 1978; Seelig 1977, 1978; Haberkorn et al. 1978; Forbes et al. 1988; Oldfield et al. 1987; Auger 2000; Macdonald et al. 2013).

Molecular dynamics simulations indicate that OmpX is surrounded by well over a full ring of phospholipids, when it's embedded in a nanodisc formed with MSP1D1Δh5 and 40 molecules of DMPC per bilayer leaflet, consistent with thermal unfolding experiments showing that these smaller nanodiscs provide a stable environment for the protein (Hagn et al. 2013). In the case of Ail, we found that MSP1D1Δh5 nanodiscs with 50 phospholipids per bilayer leaflet have the highest homogeneity and best solution NMR characteristics (Ding

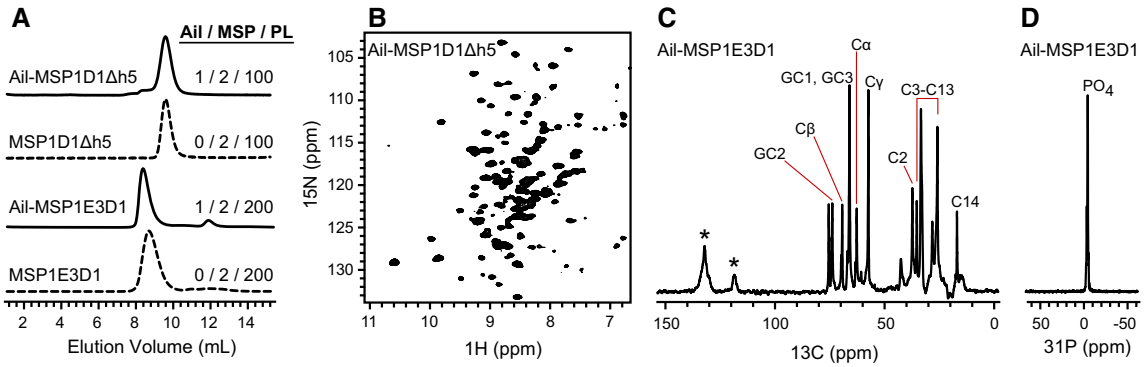

Fig. 1 Characterization of Ail nanodiscs. **A** Size exclusion chromatography of Ail nanodiscs (*solid line*) or empty nanodiscs (*dashed lines*) with optimized molar ratios of Ail to MSP to phospholipid (Ail/MSP/PL). **B** TROSY ^{1}H–^{15}N correlation NMR spectrum of ^{15}N labeled Ail in MSP1D1Δh5 nanodiscs in solution (0.5 mM Ail). **C** INEPT ^{13}C NMR spectrum of ^{13}C labeled Ail in MSP1E3D1 nanodiscs in solution (0.5 mM Ail). Assigned lipid signals were derived from published data (Oldfield and Chapman 1971; Birdsall et al. 1972; Levine et al. 1972; Haberkorn et al. 1978); *asterisks* indicate signals from protein aromatic sites. **D** Hahn echo ^{31}P-detected ^{1}H-decoupled spectrum of Ail-MSP1E3D1 nanodiscs in solution (0.5 mM Ail)

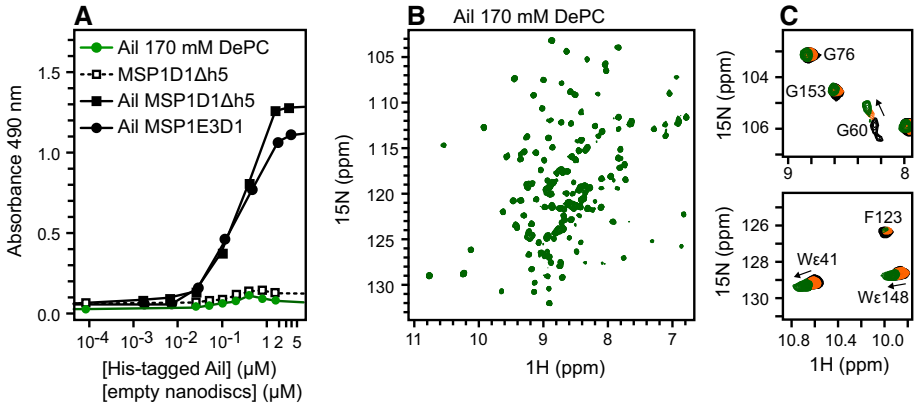

Fig. 2 Fibronectin-binding activity of Ail in nanodiscs and detergent. **A** Purified refolded Ail-His in DePC or in nanodiscs was added at increasing concentrations to fibronectin-coated plates and incubated overnight. Binding was detected by ELISA using a mouse anti-His antibody. Ail-His in MSP1D1Δh5 or MSP1E3D1 nanodiscs bind fibronectin (*black solid lines*). Ail-His in 170 mM DePC (*green*) does not bind fibronectin. Empty nanodiscs lacking Ail-His were probed with anti-ApoA1 antibody and do not bind fibronectin (*black dotted line*). Each point in each data set represents the average of three experiments. **B** TROSY ^{1}H–^{15}N correlation NMR spectrum of Ail in 170 mM DePC solution (0.5 mM Ail). **C** TROSY ^{1}H–^{15}N correlation NMR spectra of Ail in MSP1D1Δh5 nanodiscs in solution obtained in the absence of detergent (*black*), and after addition of 4 mM DePC (*orange*) or 11 mM DePC (*green*)

et al. 2015) and, since 40 lipids were sufficient for stabilizing OmpX, we conclude that 50 must also provide a stable membrane environment for Ail. For an Ail cross-barrel diameter of ~2 nm, estimated from the crystal structure (Yamashita et al. 2011), about 7 molecules of DMPC, each with a surface area of 0.6 nm^2, would be needed to form a single ring of lipids around the circumference of the barrel. The larger nanodiscs, prepared with MSP1E3D1, contained 100 phospholipid molecules per bilayer leaflet (Fig. 1), and therefore enable a membrane of 5 rings of phospholipid to form around the embedded protein. This 1/200 protein/lipid ratio is in the low range of what is typically used in solid-state NMR studies of membrane proteins in liposomes, oriented bicelles, and oriented planar bilayers (Das et al. 2013).

Ligand-binding activity of Ail in nanodiscs and effect of detergent

We next tested the ability of Ail to bind fibronectin-coated surfaces in ELISAs. The data in Fig. 2a (black) show that the fibronectin binding activity of Ail can be reconstituted in smaller MSP1D1Δh5 nanodiscs as well as the larger MSP1E3D1 nanodiscs; in both cases, Ail exhibits concentration-dependent binding to fibronectin-coated plates. The activity can be fully ascribed to Ail since assays performed with empty nanodiscs yield no ELISA signal. Conversely, no fibronectin binding is detected for Ail in 170 mM DePC (Fig. 2a, green), even though this detergent concentration is optimal for solution NMR spectroscopy, and the ^{1}H–^{15}N correlation spectrum of Ail in 170 mM DePC has narrow, homogenous resonance linewidths and large chemical shift dispersions, consistent with conformational order and relatively uniform backbone dynamics across the entire length of the polypeptide (Fig. 2b).

Recently (Ding et al. 2015), we reported that Ail adopts its native eight-stranded β-barrel fold in DePC micelles, with a conformation that is very similar to the crystal structure (Yamashita et al. 2011) and backbone dynamics that are consistent with flexibility in the functionally important extracellular loops. However, we also found that the fibronectin-binding activity is disrupted at the high detergent concentrations required for NMR studies. The data in Fig. 2c show that addition of even small amounts of DePC to Ail in nanodiscs has a profound effect on the NMR spectrum, with peaks from the water-exposed loops affected to a greater extent (Fig. 2c). For example, the signal from G60, situated in the second extracellular loop (EL2) of Ail, is perturbed by as little as 4 mM DePC, a concentration well below the critical micelle concentration of 11 mM DePC. On the other hand, signals from G76 to G153 in the transmembrane β-barrel are not highly affected. Since the extracellular loops of Ail are involved in mediating its interaction with fibronectin, the disruption of fibronectin binding in detergent micelles appears to be caused by the interaction of monomeric detergent molecules with key water-exposed sites on Ail and, possibly, also on fibronectin. Thus we conclude that although both detergents and nanodiscs support the native structure of Ail, detergents interfere with ligand binding activity, precluding parallel structure–activity correlation studies.

It is well known that detergents can have adverse effects on membrane protein structure and function (Zhou and Cross 2013). Monomeric detergent exists in equilibrium with micelles, and is sometimes found associated with crystallized membrane proteins, including Ail (Yamashita

et al. 2011). Recent studies have shown that the extracellular loops of outer membrane β-barrels are more susceptible to the surrounding environment than their transmembrane regions. For example, the detergent environment has been reported to affect the structures and dynamics of the water-exposed loops of OmpX, OmpA and Opa to greater extent than their membrane-embedded β-barrels (Hagn et al. 2013; Susac et al. 2014; Fox et al. 2014).

Small nanodiscs prepared with MSP1D1Δh5 and MSP1D1 have been used for solution NMR studies of membrane proteins, including structure determination of the outer membrane proteins OmpX and OmpA (Hagn et al. 2013; Susac et al. 2014). Nanodiscs are detergent-free and provide a soluble phospholipid bilayer environment that retains the essential anisotropic physical and chemical properties of biological membranes (Ritchie et al. 2009). Furthermore, compared to spherical liposomes, the open configuration of nanodiscs facilitates structure–activity studies where the addition of ligands is detected by direct spectroscopic comparisons.

However, nanodisc samples may not be generally suitable for solution NMR studies of all membrane proteins, and are likely to be inappropriate for chemical shift mapping studies with Ail and its high molecular weight human ligands, such as fibronectin. While the increased size of such complexes may be prohibitive for solution NMR spectroscopy, solid-state NMR has no physical size limitations and can be used with larger or motionally restricted lipid bilayer assemblies for structure–activity studies of membrane proteins in detergent-free native-like samples.

Solid-state NMR of sedimented Ail nanodiscs

We first tested sedimentation of ^{15}N labeled Ail in the MSP1D1Δh5 nanodiscs that yield high-resolution solution NMR spectra at the relatively dilute concentration of 0.5 mM Ail. Rather then attempting to sediment the sample in situ, as described originally by Bertini and coworkers (Bertini et al. 2011), we centrifuged the sample before transferring it to the MAS rotor, as described (Bertini et al. 2012b; Gardiennet et al. 2012), so as to obtain a higher concentration of isotopically labeled protein for NMR.

Centrifugation in the A/100-30 rotor of a Beckman Airfuge at 160,000×g, for 4 h yielded a dense viscous, visually transparent sediment in the bottom 50 μL fraction of the 240 μL centrifuge tube, overlaid by a fluid top fraction with the consistency of water. When this sedimented fraction was transferred to the MAS rotor for solid-state NMR experiments, abundant ^{15}N signal could be detected by ^{1}H CP with a slow spinning frequency of 5 kHz (Fig. 3a). However, no signal was detected with an

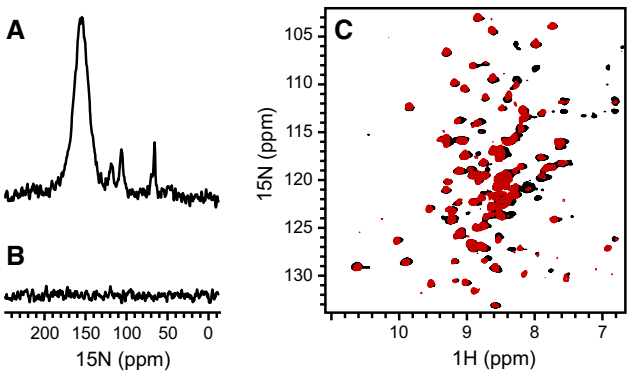

Fig. 3 NMR spectra of Ail-MSP1D1Δh5 nanodiscs obtained after sedimentation (**A**, **B**) and subsequent redilution (**C**). (**A**, **B**) Solid-state NMR ^{15}N spectra of sedimented Ail nanodiscs obtained with CP (**A**) or INEPT (**B**) under 5 kHz MAS, at 25 °C. **C** TROSY ^{1}H–^{15}N correlation solution NMR spectra obtained for Ail nanodiscs before sedimentation (*black*; 0.5 mM Ail) and after re-dilution of the sedimented sample (*red*; 0.5 mM Ail) at 45 °C

INEPT experiment (Fig. 3b). INEPT pulse sequences have been used to detect fast lipid and protein dynamics (Andronesi et al. 2005; Warschawski and Devaux 2005). Therefore, the data in Fig. 3 indicate that the rotational motion of the nanodiscs is sufficiently restricted for solid-state NMR studies.

Dilution of the sedimented fraction back to the original 0.5 mM concentration yielded a solution NMR ^{1}H/^{15}N spectrum that is essentially identical to the original spectrum obtained prior to centrifugation (Fig. 3c). This result, together with the transparent appearance of the sample after sedimentation, leads us to conclude that concentration of the Ail-MSP1D1Δh5 nanodiscs is not due to nonspecific precipitation or aggregation but rather to sedimentation under the high G forces of the centrifuge.

Encouraged by this result we performed a similar experiment with ^{13}C labeled Ail incorporated in the larger MSP1E3D1 nanodiscs. As observed for the smaller nanodiscs, centrifugation at 160,000×g, for 18 h yielded a transparent, viscous sediment at the bottom of the centrifuge tube. UV absorbance measurements indicate that the bottom 50 μL fraction is enriched in protein by a factor of 22 compared to the top fluid fraction (Table 1).

This sedimented fraction gave an excellent one dimensional ^{13}C MAS solid-state NMR spectrum by through-space ^{1}H–^{13}C CP (Fig. 4a). On the other hand, through-bond transfer of polarization by INEPT gave a ^{13}C spectrum that contains only signals from the natural abundance ^{13}C in the phospholipids (Fig. 4b), and is essentially identical to the ^{13}C INEPT spectrum of the diluted nanodiscs observed by solution NMR without MAS (Fig. 1c). The ^{31}P NMR spectrum of this sedimented fraction (Fig. 4c) now displays the powder pattern characteristic of

Table 1 Sedimentation efficiency of nanodisc samples

Sample	Initial sample		Top fraction[a]		Sedimented fraction[a]		% Enrichment in sedimented fraction
	V_i (μL)	A_{280-i}	V_{top} (μL)	$A_{280-top}$	V_{sed} (μL)	$A_{280-sed}$	
MSP1D1Δh5	200	0.891	150	0.890	50	0.89	0
Ail-MSP1D1Δh5	220	0.331	170	0.095	50	0.96	71
MSP1E3D1	135	0.550	90	0.433	45	0.73	21
Ail-MSP1E3D1	200	0.643	150	0.104	50	n.d.	84

[a] Measurements were made after centrifugation in the A/100-30 rotor of a Beckman Airfuge (90,000 rpm, room temperature, 18 h)

n.d. not determined (Value)

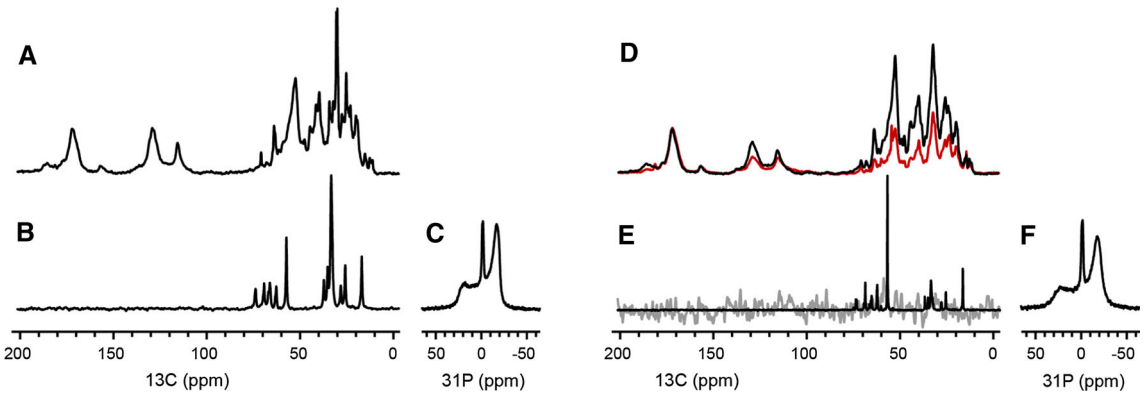

Fig. 4 One-dimensional solid-state NMR spectra of sedimented Ail-MSP1E3D1 nanodiscs (5.5 mM Ail) obtained at 25 °C (**A**–**C**) or 10 °C (**D**–**F**). (**A**, **D**) MAS (10 kHz) ^{13}C spectra obtained using CP (*black*) or DP (*red*). (**B**, **E**) ^{13}C spectra obtained using INEPT with (*black*) or without (*gray*) 10 kHz MAS. (**C**, **F**) ^{31}P spectra obtained with DP for static sample. Isotropic signal intensity (~0 ppm) is attributed to the presence of Na phosphate in the NMR buffer

liquid crystalline phospholipids in a bilayer arrangement (additional signal at the isotropic ^{31}P chemical shift frequency arises from Na phosphate in the NMR buffer), further confirming that the rotational motion of the sedimented nanodiscs is sufficiently restricted to enable observation by solid-state NMR spectroscopy.

Similar experiments performed at 10 °C, show that the CP spectrum (Fig. 4d, black) is enhanced by a factor of 2 compared to its counterpart obtained by direct ^{13}C polarization (Fig. 4d, red), further indicating that the dipolar interactions are not averaged by fast rotational motions and can be exploited to enhance the NMR signal by CP, as intended (Pines et al. 1973). The broadening seen at the edges of the ^{31}P powder pattern acquired at 10 °C (Fig. 4f) is consistent with the phospholipid bilayer transition from liquid crystalline to gel phase, which occurs at 23 °C for DMPC and DMPG. Thus, the data show that the sedimented nanodiscs are motionally restricted and exhibit the expected properties of intact well-behaved phospholipid bilayers.

Furthermore, the two-dimensional ^{13}C correlation spectrum (Fig. 5) shows that Ail maintains its structure in the sedimented Ail MSP1E3D1 nanodiscs. The spectrum, obtained at 27 °C, above the phase transition of the lipids DMPC and DMPG, displays several resolved peaks from ^{13}C labeled Ail, as well as intense diagonal intensity from the natural abundance ^{13}C of the lipids. Equally good spectra were obtained at 27, 5 and 0 °C.

The spectral resolution is comparable to that obtained with Ail in proteoliposomes at 0 °C (Ding et al. 2013), with many peaks at identical or similar positions. However, while the spectrum of Ail in sedimented nanodiscs was obtained with 32 scans (18 h acquisition), the spectrum from liposomes was obtained with 512 scans (42 h acquisition), due to the lower concentration of Ail in the latter. It is possible that the open geometry of nanodiscs affords greater extent of sample concentration and greater filling factor than spherical liposomes, a potentially important benefit associated with their use in NMR experiments.

In the ^{13}C correlation spectrum, peaks from the Ala, Ile, Pro, Ser, and Thr residues are detected at chemical shifts consistent with β-sheet conformation, and several of these signals are well resolved. Comparison with the Cα–Cβ peak positions derived from the chemical shifts assigned in the solution NMR spectrum of Ail in DePC micelles

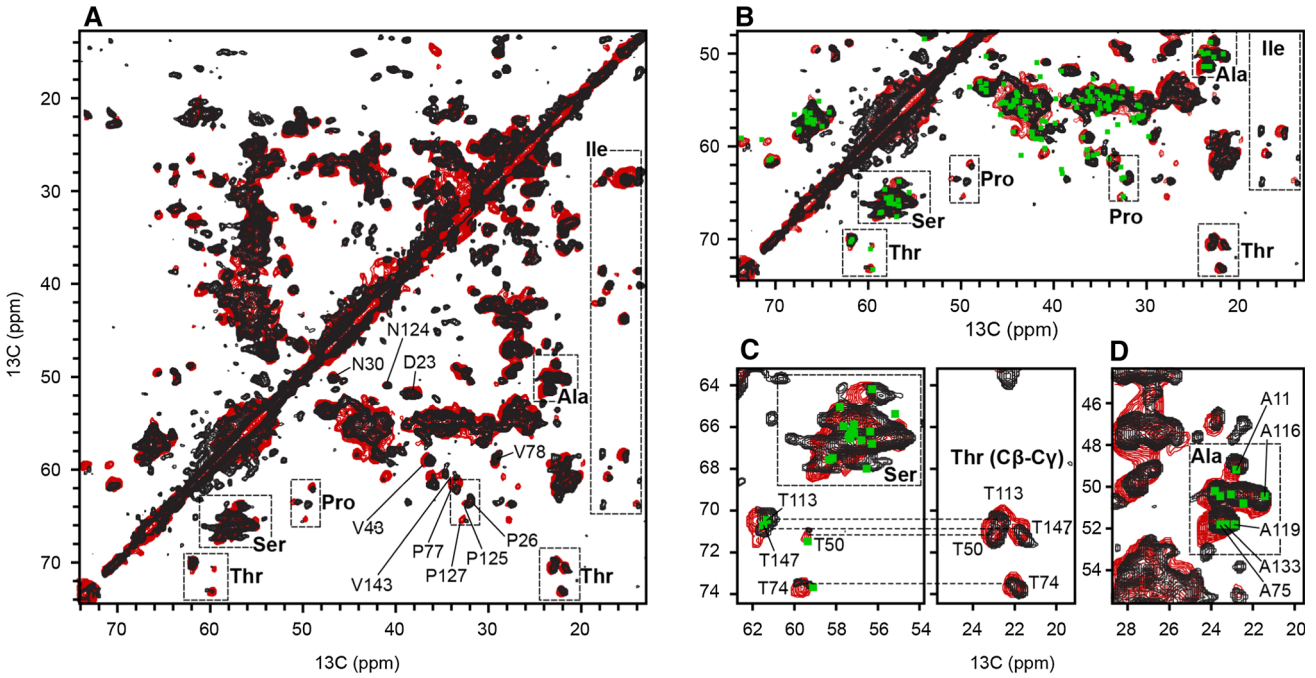

Fig. 5 Two-dimensional solid-state NMR ^{13}C correlation spectra of Ail in sedimented MSP1E3D1 nanodiscs (*black*; 5.5 mM Ail) or proteoliposomes (*red*; 2.4 mM Ail). Spectra were recorded at 27 °C (for sedimented nanodiscs) or 0 °C (for liposomes), with 10 kHz MAS, using PDSD with 32 scans for sedimented nanodiscs or 512 scans for liposomes. **A** *Boxes* highlight signals with chemical shifts characteristic for Ala, Ile, Pro and Thr residues. **B** Selected region of the spectra showing the Cα–Cβ correlations derived from the assigned spectrum of Ail in 170 mM DePC (*green*). (**C**, **D**) Expanded regions of the spectra

(Fig. 5b) reveals many similarities, demonstrating that the protein adopts the same overall structure in detergent as in lipid bilayers.

Expanded regions of the spectrum show that several peaks can be tentatively assigned by direct comparison with the solution NMR spectrum of Ail in DePC (Fig. 5c). For example, peaks from Cβ–Cα and Cβ–Cγ correlations are observed for all four Thr residues in the protein, and can be tentatively assigned from the corresponding solution NMR resonances. All four Thr Cβ–Cγ peaks have similar intensities. However, the intensities of the Cβ–Cα peaks vary, with strong signals observed for T113 and T147, located in transmembrane β-strands β6 and β8, and weaker signals for T50 in the second extracellular loop and T74 in transmembrane β4.

Similarly, peaks from Cβ–Cα and Cδ–Cα correlations of the four Pro residues can be clearly resolved and tentatively assigned, as can several Cβ–Cα signals from the nine Ala residues (Fig. 5d). The positions of Cβ–Cα peaks from the sixteen Ser residues also correlate well with their solution NMR chemical shifts measured in DePC (Fig. 5c). Furthermore, peaks correlating Cδ and Cγ to Cβ side chain sites are detected for the seven Ile residues of Ail (Fig. 5a). The ability to resolve peaks from extracellular loop sites (e.g. T50, D23) will be particularly useful for chemical shift mapping experiments aimed at characterizing the interactions of Ail with its ligands.

Sedimentation properties of nanodiscs

As described by Bertini and coworkers (Bertini et al. 2011, 2012a), it is possible to estimate the sedimentation properties of a molecular species in a solvent using equations derived over the years by the large field of protein ultracentrifugation (Laue and Stafford 1999). To understand the sedimentation behavior of nanodiscs, we used these equations to calculate various hydrodynamic parameters (Table 2). The time (t_{SED}) required for sedimentation was estimated using the Svedberg equation, $t_{SED} = 2.533 \times 10^{11}$ (k/S), where the k factor reflects the rotor's pelleting efficiency and depends on the rotor's geometry and angular velocity, while the sedimentation coefficient, S, depends on the hydrodynamic properties of the nanodisc assembly.

The air-driven centrifuge rotor that we used to obtain nanodisc sedimentation has a very favorable pelleting efficiency, with a k factor of 21.7 achieved at 90,000 rpm (160,000×*g*), near the rotor's maximum angular velocity of 92,000 rpm. Furthermore, the small 240 µL volume of each of the six centrifuge tubes that fit the rotor helps minimize sample loss. The value of S for each nanodisc was derived from the known hydrodynamic properties of proteins and lipids in water, the stoichiometry and molecular weights of the protein and lipid nanodisc components, and measurements of the hydrodynamic radii of MSP1D1Δh5 and

Table 2 Calculated sedimentation properties of empty and Ail-containing nanodiscs

	MSP1D1Δh5	Ail-MSP1D1Δh5	MSP1E3D1	Ail-MSP1E3D1
n_{Ail}	0	1	0	1
n_{MSP}	2	2	2	2
n_{PC}	70	70	140	140
n_{PG}	30	30	60	60
M_n(g/mol)[a]	107,097	124,688	196,205	213,797
ν_n(mL/g)[b]	0.92	0.90	0.93	0.92
M_B(g/mol)[c]	7,431	10,402	11,824	14,795
R_h(nm)[d]	4.6	4.6	7.0	7.0
f(g/sec)[e]	0.89×10^{-7}	0.89×10^{-7}	1.35×10^{-7}	1.35×10^{-7}
S(S)[f]	1.35	1.89	1.41	1.76
t_{SED}(hr)[g]	16.1	11.5	15.4	12.3

[a] The molecular weight of the nanodisc (M_n) was estimated from the number of molecules (n) and molecular weights (M) of the individual protein and lipids in the nanodisc, as: $M_n = n_{Ail}\, M_{Ail} + n_{MSP}\, M_{MSP} + n_{PC}\, M_{DMPC} + n_{PG}\, M_{DMPG}$, where M_{Ail} = 17,592 Da; $M_{MSP1D1\Delta h5}$ = 19,488 Da; $M_{MSP1E3D1}$ = 29,982 Da; M_{DMPC} = 678 Da and M_{DMPG} = 689 Da

[b] The partial specific volume of the nanodisc (ν_n) was estimated from the partial specific volumes of protein (ν_p = 0.82 mL/g) (Ferella et al. 2013), DPMC (ν_{DMPC} = 0.98 mL/g) (Nagle and Tristram-Nagle 2000) and DMPG (ν_{DMPG} = 0.94 mL/g) (Pan et al. 2012), as: $\nu_n = (\nu_p - n_{Ail}\, M_{Ail} + \nu_p\, n_{MSP}\, M_{MSP} + \nu_{DMPC}\, n_{PC}\, M_{DMPC} + \nu_{DMPG}\, n_{PG}\, M_{DMPG})/M_n$

[c] The buoyant mass of the nanodisc (M_B) was estimated from M_n, ν_n and the solvent's density (ρ_{sol} = 1.014 g/mL), as: $M_B = M_n\,(1 - \nu_n\, \rho_{sol})$. The value of ρ_{sol} for NMR buffer was estimated using the SEDNTERP software

[d] Values of the hydrodynamic radius (R_h) were taken from experimental size exclusion chromatography analyses of MSP1D1Δh5 (Hagn et al. 2013) and MSP1E3D1 (Denisov et al. 2007) nanodiscs

[e] The frictional coefficient (f) was derived from R_h and the viscosity of the solvent (η_{sol} = 0.01 g/mL), as: $f = 6\pi\, \eta_{sol}\, R_h$. The value of η_{sol} for NMR buffer was estimated using the SEDNTERP software

[f] The sedimentation coefficient (S) was estimated from Avogadro's number (N_A), M_B and f, as: $S = (M_B/f) \times (10^{13}/N_A)$, where the factor $10^{13}/N_A$ yields S in Svedberg units (S), defined as $1S = 10^{-13}$ s

[g] $t_{SED} = 2.533 \times 10^{11}$ (k/S), where k = 21.7 for the A-100/30 Beckman Airfuge rotor

MSP1E3D1 nanodiscs obtained by size exclusion chromatography (Hagn et al. 2013; Denisov et al. 2007).

Although the values in Table 2 are theoretical, they are well within the range observed experimentally in analytical centrifugation experiments with lipid nanodiscs. The estimates of partial specific volume (ν_n) agree with data reported by Sykes and coworkers on ApoE3-DMPG lipoparticles (Raussens et al. 2000) and by Grisshammer and coworkers on MSP1D1 nanodiscs (Inagaki et al. 2013).

The hydrodynamic properties of lipid assemblies are governed by phospholipid composition, as the specific nature of hydrocarbon chains and polar headgroups influence the partial specific volumes of phospholipids. The estimates in Table 2 illustrate how the sedimentation properties of nanodiscs are affected, not only by the molecular weight of the entire assembly, but also, significantly, by the higher specific volume (low density), relative to protein, of the lipid molecules in the bilayer. It is the balance of these properties that determines whether the species will sediment, float or remain dispersed solution.

In both MSP1D1Δh5 and MSP1E3D1 nanodiscs the incorporation of Ail decreases the overall specific volumes and the predicted sedimentation times. The sedimentation efficiency will be further enhanced by the addition of ligands that bind the nanodisc-embedded protein, such as fibronectin, in the case of Ail. The trend of these theoretical predictions are in line with our observations (Table 1) that Ail-containing MSP1D1Δh5 nanodiscs could be sedimented by Airfuge centrifugation, while their empty counterparts could not.

Conclusions

In summary, our results show that nanodiscs containing the outer membrane protein Ail can be sedimented by centrifugation and transferred to a rotor for solid-state NMR experiments. The nanodisc samples can be diluted back to their original concentration for solution NMR studies, indicating that neither the protein or lipid bilayer structures are disrupted by sedimentation. Furthermore, since the protein is active in the nanodiscs the same samples can be used for activity assays, solution NMR and solid-state NMR experiments, facilitating investigation of the structure and activity properties across a wide range of

dynamics time scales, without having to add potentially damaging detergents or precipitants, and without the need to lyophilize the sample.

Acknowledgments We thank Bibhuti Das, Chris Grant, Chin Wu and Stan Opella for assistance with solid-state NMR experiments. This research was supported by Grants from the National Institutes of Health (GM100265; P41 EB002031; P30 CA030199).

References

Andronesi OC, Becker S, Seidel K, Heise H, Young HS, Baldus M (2005) Determination of membrane protein structure and dynamics by magic-angle-spinning solid-state NMR spectroscopy. J Am Chem Soc 127(37):12965–12974. doi:10.1021/ja0530164

Arora A, Tamm LK (2001) Biophysical approaches to membrane protein structure determination. Curr Opin Struct Biol 11(5):540–547. doi:10.1016/S0959-440X(00)00246-3

Auger M (2000) Biological membrane structure by solid-state NMR. Curr Issues Mol Biol 2(4):119–124

Berardi MJ, Shih WM, Harrison SC, Chou JJ (2011) Mitochondrial uncoupling protein 2 structure determined by NMR molecular fragment searching. Nature 476(7358):109–113. doi:10.1038/nature10257

Bertini I, Luchinat C, Parigi G, Ravera E, Reif B, Turano P (2011) Solid-state NMR of proteins sedimented by ultracentrifugation. Proc Natl Acad Sci USA 108(26):10396–10399. doi:10.1073/pnas.1103854108

Bertini I, Engelke F, Gonnelli L, Knott B, Luchinat C, Osen D, Ravera E (2012a) On the use of ultracentrifugal devices for sedimented solute NMR. J Biomol NMR 54(2):123–127. doi:10.1007/s10858-012-9657-y

Bertini I, Engelke F, Luchinat C, Parigi G, Ravera E, Rosa C, Turano P (2012b) NMR properties of sedimented solutes. Phys Chem Chem Phys 14(2):439–447. doi:10.1039/c1cp22978h

Bibow S, Carneiro MG, Sabo TM, Schwiegk C, Becker S, Riek R, Lee D (2014) Measuring membrane protein bond orientations in nanodiscs via residual dipolar couplings. Protein Sci. doi:10.1002/pro.2482

Birdsall NJM, Feeney J, Lee AG, Levine YK, Metcalfe JC (1972) Dipalmitoyl-lecithin: assignment of the 1H and 13C nuclear magnetic resonance spectra, and conformational studies. J Chem Soc Perkin Trans 2(10):1441–1445. doi:10.1039/P29720001441

Bloom M, Burnell EE, Roeder SBW, Valic MI (1977) Nuclear magnetic resonance line shapes in lyotropic liquid crystals and related systems. J Chem Phys 66(7):3012–3020. doi:10.1063/1.434314

Bloom M, Burnell EE, MacKay AL, Nichol CP, Valic MI, Weeks G (1978) Fatty acyl chain order in lecithin model membranes determined from proton magnetic resonance. Biochemistry 17(26):5750–5762. doi:10.1021/bi00619a024

Boettcher JM, Davis-Harrison RL, Clay MC, Nieuwkoop AJ, Ohkubo YZ, Tajkhorshid E, Morrissey JH, Rienstra CM (2011) Atomic view of calcium-induced clustering of phosphatidylserine in mixed lipid bilayers. Biochemistry 50(12):2264–2273. doi:10.1021/bi1013694

Burnell EE, Cullis PR, de Kruijff B (1980) Effects of tumbling and lateral diffusion on phosphatidylcholine model membrane 31P-NMR lineshapes. Biochim Biophys Acta 603(1):63–69

Chill JH, Louis JM, Delaglio F, Bax A (2007) Local and global structure of the monomeric subunit of the potassium channel KcsA probed by NMR. Biochim Biophys Acta 1768(12):3260–3270. doi:10.1016/j.bbamem.2007.08.006

Das N, Murray DT, Cross TA (2013) Lipid bilayer preparations of membrane proteins for oriented and magic-angle spinning solid-state NMR samples. Nat Protoc 8(11):2256–2270. doi:10.1038/nprot.2013.129

Delaglio F, Grzesiek S, Vuister GW, Zhu G, Pfeifer J, Bax A (1995) NMRPipe: a multidimensional spectral processing system based on UNIX pipes. J Biomol NMR 6(3):277–293

Denisov IG, Baas BJ, Grinkova YV, Sligar SG (2007) Cooperativity in cytochrome P450 3A4: linkages in substrate binding, spin state, uncoupling, and product formation. J Biol Chem 282(10):7066–7076. doi:10.1074/jbc.M609589200

Ding Y, Fujimoto LM, Yao Y, Plano GV, Marassi FM (2015) Influence of the lipid membrane environment on structure and activity of the outer membrane protein Ail from *Yersinia pestis*. Biochim Biophys Acta 1848(2):712–720. doi:10.1016/j.bbamem.2014.11.021

Ding Y, Yao Y, Marassi FM (2013) Membrane protein structure determination in membrana. Acc Chem Res 46(9):2182–2190. doi:10.1021/ar400041a

Drechsler A, Separovic F (2003) Solid-state NMR structure determination. IUBMB Life 55(9):515–523. doi:10.1080/15216540310001622740

Durr UH, Gildenberg M, Ramamoorthy A (2012) The magic of bicelles lights up membrane protein structure. Chem Rev 112(11):6054–6074. doi:10.1021/cr300061w

Etzkorn M, Raschle T, Hagn F, Gelev V, Rice AJ, Walz T, Wagner G (2013) Cell-free expressed bacteriorhodopsin in different soluble membrane mimetics: biophysical properties and NMR accessibility. Structure 21(3):394–401. doi:10.1016/j.str.2013.01.005

Ferella L, Luchinat C, Ravera E, Rosato A (2013) SedNMR: a web tool for optimizing sedimentation of macromolecular solutes for SSNMR. J Biomol NMR 57(4):319–326. doi:10.1007/s10858-013-9795-x

Fernandez C, Wuthrich K (2003) NMR solution structure determination of membrane proteins reconstituted in detergent micelles. FEBS Lett 555(1):144–150

Forbes J, Bowers J, Shan X, Moran L, Oldfield E, Moscarello MA (1988) Some new developments in solid-state nuclear magnetic resonance spectroscopic studies of lipids and biological membranes, including the effects of cholesterol in model and natural systems. J Chem Soc Faraday Trans 1 Phys Chem Condens Phases 84(11):3821–3849. doi:10.1039/F19888403821

Fox DA, Larsson P, Lo RH, Kroncke BM, Kasson PM, Columbus L (2014) The Structure of the Neisserial outer membrane protein Opa: loop flexibility essential to receptor recognition and bacterial engulfment. J Am Chem Soc. doi:10.1021/ja503093y

Franks WT, Linden AH, Kunert B, van Rossum BJ, Oschkinat H (2012) Solid-state magic-angle spinning NMR of membrane proteins and protein-ligand interactions. Eur J Cell Biol 91(4):340–348. doi:10.1016/j.ejcb.2011.09.002

Gardiennet C, Schutz AK, Hunkeler A, Kunert B, Terradot L, Bockmann A, Meier BH (2012) A sedimented sample of a 59 kDa dodecameric helicase yields high-resolution solid-state NMR spectra. Angew Chem Int Ed Engl 51(31):7855–7858. doi:10.1002/anie.201200779

Gluck JM, Wittlich M, Feuerstein S, Hoffmann S, Willbold D, Koenig BW (2009) Integral membrane proteins in nanodiscs can be studied by solution NMR spectroscopy. J Am Chem Soc 131(34):12060–12061. doi:10.1021/ja904897p

Gopinath T, Mote KR, Veglia G (2013) Sensitivity and resolution enhancement of oriented solid-state NMR: application to membrane proteins. Prog Nucl Magn Reson Spectrosc 75:50–68. doi:10.1016/j.pnmrs.2013.07.004

Haberkorn RA, Herzfeld J, Griffin RG (1978) High resolution phosphorus-31 and carbon-13 nuclear magnetic resonance spectra of unsonicated model membranes. J Am Chem Soc 100(4):1296–1298. doi:10.1021/ja00472a048

Hagn F, Etzkorn M, Raschle T, Wagner G (2013) Optimized phospholipid bilayer nanodiscs facilitate high-resolution structure determination of membrane proteins. J Am Chem Soc 135(5):1919–1925. doi:10.1021/ja310901f

Hiller S, Wagner G (2009) The role of solution NMR in the structure determinations of VDAC-1 and other membrane proteins. Curr Opin Struct Biol 19(4):396–401. doi:10.1016/j.sbi.2009.07.013

Hong M, Zhang Y, Hu F (2012) Membrane protein structure and dynamics from NMR spectroscopy. Annu Rev Phys Chem 63:1–24. doi:10.1146/annurev-physchem-032511-143731

Inagaki S, Ghirlando R, Grisshammer R (2013) Biophysical characterization of membrane proteins in nanodiscs. Methods 59(3): 287–300. doi:10.1016/j.ymeth.2012.11.006

Johnson BA, Blevins RA (1994) NMR View: a computer program for the visualization and analysis of NMR data. J Biomol NMR 4(5):603–614. doi:10.1007/BF00404272

Kijac AZ, Li Y, Sligar SG, Rienstra CM (2007) Magic-angle spinning solid-state NMR spectroscopy of nanodisc-embedded human CYP3A4. Biochemistry 46(48):13696–13703. doi:10.1021/bi701411g

Kijac A, Shih AY, Nieuwkoop AJ, Schulten K, Sligar SG, Rienstra CM (2010) Lipid-protein correlations in nanoscale phospholipid bilayers determined by solid-state nuclear magnetic resonance. Biochemistry 49(43):9190–9198. doi:10.1021/bi1013722

Kim HJ, Howell SC, Van Horn WD, Jeon YH, Sanders CR (2009) Recent advances in the application of solution NMR Spectroscopy to multi-span integral membrane Proteins. Prog Nucl Magn Reson Spectrosc 55(4):335–360. doi:10.1016/j.pnmrs.2009.07.002

Laue TM, Stafford WF 3rd (1999) Modern applications of analytical ultracentrifugation. Annu Rev Biophys Biomol Struct 28:75–100. doi:10.1146/annurev.biophys.28.1.75

Levine YK, Birdsall NJ, Lee AG, Metcalfe JC (1972) 13 C nuclear magnetic resonance relaxation measurements of synthetic lecithins and the effect of spin-labeled lipids. Biochemistry 11(8): 1416–1421

Li Y, Kijac AZ, Sligar SG, Rienstra CM (2006) Structural analysis of nanoscale self-assembled discoidal lipid bilayers by solid-state NMR spectroscopy. Biophys J 91(10):3819–3828. doi:10.1529/biophysj.106.087072

Loquet A, Habenstein B, Lange A (2013) Structural investigations of molecular machines by solid-state NMR. Acc Chem Res 46(9):2070–2079. doi:10.1021/ar300320p

Macdonald PM, Saleem Q, Lai A, Morales HH (2013) NMR methods for measuring lateral diffusion in membranes. Chem Phys Lipids 166:31–44. doi:10.1016/j.chemphyslip.2012.12.004

Maltsev S, Lorigan GA (2011) Membrane proteins structure and dynamics by nuclear magnetic resonance. Compr Physiol 1(4):2175–2187. doi:10.1002/cphy.c110022

McDermott A (2009) Structure and dynamics of membrane proteins by magic angle spinning solid-state NMR. Annu Rev Biophys 38:385–403. doi:10.1146/annurev.biophys.050708.133719

Miller VL, Beer KB, Heusipp G, Young BM, Wachtel MR (2001) Identification of regions of Ail required for the invasion and serum resistance phenotypes. Mol Microbiol 41(5):1053–1062

Morris GA, Freeman R (1979) Enhancement of nuclear magnetic resonance signals by polarization transfer. J Am Chem Soc 101(3):760–762. doi:10.1021/ja00497a058

Mors K, Roos C, Scholz F, Wachtveitl J, Dotsch V, Bernhard F, Glaubitz C (2013) Modified lipid and protein dynamics in nanodiscs. Biochim Biophys Acta 1828(4):1222–1229. doi:10.1016/j.bbamem.2012.12.011

Murray DT, Das N, Cross TA (2013) Solid state NMR strategy for characterizing native membrane protein structures. Acc Chem Res 46(9):2172–2181. doi:10.1021/ar3003442

Nagle JF, Tristram-Nagle S (2000) Structure of lipid bilayers. Biochim Biophys Acta 1469(3):159–195. doi:10.1016/S0304-4157(00)00016-2

Ni QZ, Daviso E, Can TV, Markhasin E, Jawla SK, Swager TM, Temkin RJ, Herzfeld J, Griffin RG (2013) High frequency dynamic nuclear Polarization. Acc Chem Res 46(9):1933–1941. doi:10.1021/ar300348n

Oldfield E, Chapman D (1971) Carbon-13 pulse Fourier transform NMR of lecithins. Biochem Biophys Res Commun 43(5): 949–953

Oldfield E, Bowers JL, Forbes J (1987) High-resolution proton and carbon-13 NMR of membranes: why sonicate? Biochemistry 26(22):6919–6923

Orwick-Rydmark M, Lovett JE, Graziadei A, Lindholm L, Hicks MR, Watts A (2012) Detergent-free incorporation of a seven-trans-membrane receptor protein into nanosized bilayer Lipodisq particles for functional and biophysical studies. Nano Lett 12(9): 4687–4692. doi:10.1021/nl3020395

Pan J, Heberle FA, Tristram-Nagle S, Szymanski M, Koepfinger M, Katsaras J, Kucerka N (2012) Molecular structures of fluid phase phosphatidylglycerol bilayers as determined by small angle neutron and X-ray scattering. Biochim Biophys Acta 1898(9): 2135–2148. doi:10.1016/j.bbamem.2012.05.007

Park SH, Berkamp S, Cook GA, Chan MK, Viadiu H, Opella SJ (2011) Nanodiscs versus macrodiscs for NMR of membrane proteins. Biochemistry 50(42):8983–8985. doi:10.1021/bi201289c

Park SH, Das BB, Casagrande F, Tian Y, Nothnagel HJ, Chu M, Kiefer H, Maier K, De Angelis A, Marassi FM, Opella SJ (2012) Structure of the chemokine receptor CXCR1 in phospholipid bilayers. Nature 491(7426):779–783. doi:10.1038/nature11580

Pervushin K, Riek R, Wider G, Wuthrich K (1997) Attenuated T2 relaxation by mutual cancellation of dipole-dipole coupling and chemical shift anisotropy indicates an avenue to NMR structures of very large biological macromolecules in solution. Proc Natl Acad Sci USA 94(23):12366–12371

Pines A, Gibby MG, Waugh JS (1973) Proton-enhanced NMR of dilute spins in solids. J Chem Phys 59:569–590

Plesniak LA, Mahalakshmi R, Rypien C, Yang Y, Racic J, FM Marassi (2011) Expression, refolding, and initial structural characterization of the *Y. pestis* Ail outer membrane protein in lipids. Biochim Biophys Acta 1808(1):482–489. doi:10.1016/j.bbamem.2010.09.017

Poget SF, Girvin ME (2007) Solution NMR of membrane proteins in bilayer mimics: small is beautiful, but sometimes bigger is better. Biochim Biophys Acta 1768(12):3098–3106. doi:10.1016/j.bbamem.2007.09.006

Prosser RS, Evanics F, Kitevski JL, Patel S (2007) The measurement of immersion depth and topology of membrane proteins by solution state NMR. Biochim Biophys Acta 1768(12):3044–3051. doi:10.1016/j.bbamem.2007.09.011

Raschle T, Hiller S, Yu TY, Rice AJ, Walz T, Wagner G (2009) Structural and functional characterization of the integral membrane protein VDAC-1 in lipid bilayer nanodiscs. J Am Chem Soc 131(49):17777–17779. doi:10.1021/ja907918r

Raussens V, Mah MK, Kay CM, Sykes BD, Ryan RO (2000) Structural characterization of a low density lipoprotein receptor-active apolipoprotein E peptide, ApoE3-(126–183). J Biol Chem 275(49):38329–38336. doi:10.1074/jbc.M005732200

Ritchie TK, Grinkova YV, Bayburt TH, Denisov IG, Zolnerciks JK, Atkins WM, Sligar SG (2009) Reconstitution of membrane proteins in phospholipid bilayer nanodiscs. Methods Enzymol 464:211–231. doi:10.1016/S0076-6879(09)64011-8

Sackett K, Nethercott MJ, Zheng Z, Weliky DP (2014) Solid-state NMR spectroscopy of the HIV gp41 membrane fusion protein supports intermolecular antiparallel beta sheet fusion peptide

structure in the final six-helix bundle state. J Mol Biol 426(5):1077–1094. doi:10.1016/j.jmb.2013.11.010
Salzmann M, Pervushin K, Wider G, Senn H, Wuthrich K (1998) TROSY in triple-resonance experiments: new perspectives for sequential NMR assignment of large proteins. Proc Natl Acad Sci USA 95(23):13585–13590
Sanders CR, Sonnichsen F (2006) Solution NMR of membrane proteins: practice and challenges. Magn Reson Chem 44(S1): S24–S40
Seelig J (1977) Deuterium magnetic resonance: theory and application to lipid membranes. Q Rev Biophys 10(3):353–418
Seelig J (1978) 31P nuclear magnetic resonance and the head group structure of phospholipids in membranes. Biochim Biophys Acta 515(2):105–140
Sharma M, Yi M, Dong H, Qin H, Peterson E, Busath DD, Zhou HX, Cross TA (2010) Insight into the mechanism of the influenza a proton channel from a structure in a lipid bilayer. Science 330(6003):509–512. doi:10.1126/science.1191750
Shenkarev ZO, Lyukmanova EN, Solozhenkin OI, Gagnidze IE, Nekrasova OV, Chupin VV, Tagaev AA, Yakimenko ZA, Ovchinnikova TV, Kirpichnikov MP, Arseniev AS (2009) Lipid-protein nanodiscs: possible application in high-resolution NMR investigations of membrane proteins and membrane-active peptides. Biochem Mosc 74(7):756–765
Shenkarev ZO, Lyukmanova EN, Paramonov AS, Shingarova LN, Chupin VV, Kirpichnikov MP, Blommers MJ, Arseniev AS (2010) Lipid-protein nanodiscs as reference medium in detergent screening for high-resolution NMR studies of integral membrane proteins. J Am Chem Soc 132(16):5628–5629. doi:10.1021/ja9097498
Shenkarev ZO, Lyukmanova EN, Butenko IO, Petrovskaya LE, Paramonov AS, Shulepko MA, Nekrasova OV, Kirpichnikov MP, Arseniev AS (2013) Lipid-protein nanodiscs promote in vitro folding of transmembrane domains of multi-helical and multimeric membrane proteins. Biochim Biophys Acta 1828(2): 776–784. doi:10.1016/j.bbamem.2012.11.005
Shuker SB, Hajduk PJ, Meadows RP, Fesik SW (1996) Discovering high-affinity ligands for proteins: SAR by NMR. Science 274(5292):1531–1534
Susac L, Horst R, Wuthrich K (2014) Solution-NMR characterization of outer-membrane protein A from *E. coli* in lipid bilayer nanodiscs and detergent micelles. ChemBioChem 15(7):995–1000. doi:10.1002/cbic.201300729
Szeverenyi NM, Sullivan MJ, Maciel GE (1982) Observation of spin exchange by two-dimensional Fourier transform ^{13}C cross-polarization-magic angle spinning. J Magn Reson 47:462–475
Tamm LK, Hong H, Liang B (2004) Folding and assembly of beta-barrel membrane proteins. Biochim Biophys Acta 1666(1–2):250–263
Tang M, Comellas G, Rienstra CM (2013) Advanced solid-state NMR approaches for structure determination of membrane proteins and amyloid fibrils. Acc Chem Res 46(9):2080–2088. doi:10.1021/ar4000168
Teriete P, Franzin CM, Choi J, Marassi FM (2007) Structure of the Na, K-ATPase regulatory protein FXYD1 in micelles. Biochemistry 46(23):6774–6783. doi:10.1021/bi700391b
Tsang TM, Felek S, Krukonis ES (2010) Ail binding to fibronectin facilitates Yersinia pestis binding to host cells and Yop delivery. Infect Immun 78(8):3358–3368. doi:10.1128/IAI.00238-10
Tsang TM, Annis DS, Kronshage M, Fenno JT, Usselman LD, Mosher DF, Krukonis ES (2012) Ail protein binds ninth type III fibronectin repeat (9FNIII) within central 120-kDa region of fibronectin to facilitate cell binding by Yersinia pestis. J Biol Chem 287(20):16759–16767. doi:10.1074/jbc.M112.358978
Tsang TM, Wiese JS, Felek S, Kronshage M, Krukonis ES (2013) Ail proteins of *Yersinia pestis* and *Y. pseudotuberculosis* have different cell binding and invasion activities. PLoS ONE 8(12):e83621. doi:10.1371/journal.pone.0083621
Tzitzilonis C, Eichmann C, Maslennikov I, Choe S, Riek R (2013) Detergent/nanodisc screening for high-resolution NMR studies of an integral membrane protein containing a cytoplasmic domain. PLoS ONE 8(1):e54378. doi:10.1371/journal.pone.0054378
Ullrich SJ, Glaubitz C (2013) Perspectives in enzymology of membrane proteins by solid-state NMR. Acc Chem Res 46(9):2164–2171. doi:10.1021/ar4000289
Wang Y, Tjandra N (2013) Structural insights of tBid, the caspase-8-activated Bid, and its BH3 domain. J Biol Chem 288(50):35840–35851. doi:10.1074/jbc.M113.503680
Wang S, Munro RA, Shi L, Kawamura I, Okitsu T, Wada A, Kim SY, Jung KH, Brown LS, Ladizhansky V (2013) Solid-state NMR spectroscopy structure determination of a lipid-embedded heptahelical membrane protein. Nat Methods 10(10):1007–1012. doi:10.1038/nmeth.2635
Warschawski DE. http://www.drorlist.com/nmr.html
Warschawski DE, Devaux PF (2005) 1H–13C Polarization transfer in membranes: a tool for probing lipid dynamics and the effect of cholesterol. J Magn Reson 177(1):166–171. doi:10.1016/j.jmr.2005.07.011
Weingarth M, Baldus M (2013) Solid-state NMR-based approaches for supramolecular structure elucidation. Acc Chem Res 46(9): 2037–2046. doi:10.1021/ar300316e
Yamashita S, Lukacik P, Barnard TJ, Noinaj N, Felek S, Tsang TM, Krukonis ES, Hinnebusch BJ, Buchanan SK (2011) Structural insights into Ail-mediated adhesion in *Yersinia pestis*. Structure 19(11):1672–1682. doi:10.1016/j.str.2011.08.010
Zhou HX, Cross TA (2013) Influences of membrane mimetic environments on membrane protein structures. Annu Rev Biophys 42:361–392. doi:10.1146/annurev-biophys-083012-130326
Zhou Y, Cierpicki T, Jimenez RH, Lukasik SM, Ellena JF, Cafiso DS, Kadokura H, Beckwith J, Bushweller JH (2008) NMR solution structure of the integral membrane enzyme DsbB: functional insights into DsbB-catalyzed disulfide bond formation. Mol Cell 31(6):896–908. doi:10.1016/j.molcel.2008.08.028